ELSEVIER

Catalysis Today 53 (1999) 177–188

CATALYSIS TODAY

www.elsevier.com/locate/cattod

Kinetic simulation of ammonia synthesis catalyzed by ruthenium

O. Hinrichsen *

Ruhr-Universität Bochum, Lehrstuhl für Technische Chemie, D-44780 Bochum, Germany

Abstract

Microkinetic analysis is a powerful tool for elucidating the catalytic surface chemistry of a variety of reactions. Starting with a detailed description of the elementary reaction steps, a thorough quantitative microkinetic analysis of the transient and steady-state experiments is performed. The resulting microkinetic models can be used to bridge the *pressure and material gaps* between results collected on well-defined single crystals under ultra-high vacuum conditions and on supported-metal commercial catalysts under industrial conditions. This approach will be presented for the ammonia synthesis reaction catalyzed by ruthenium. The reasons that this microkinetic analysis works so well will be explored in this contribution.

Keywords: Microkinetic analysis; Mesoscopic modeling; NH_3 synthesis; Ru catalysts; Transient kinetics; Steady-state kinetics

1. Introduction

The synthesis of ammonia from hydrogen and nitrogen is part of one of the most important processes in the chemical industry. After sulfuric acid, ammonia accounts for the second largest inorganic chemical production. Produced by the Haber–Bosch process, most ammonia is used for manufacture of agricultural fertilizer [1]. The current annual world capacity for the industrial production of ammonia exceeds 130 million tons with a yearly increase of approximately 2% [2].

In order to optimize the reaction conditions of an applied chemical process, and to provide new guidelines for catalyst design, a basic understanding of the catalytic chemistry on the catalyst surface is necessary. In the last decade, microkinetic analysis has turned into a valuable tool for unraveling reaction mechanisms in heterogeneous catalysis and for evaluation of kinetic parameters of the elementary steps on a *mesoscopic* level [3]. In the microkinetic approach, the kinetic model for a catalytic reaction is formulated with kinetic parameters which are physical meaningful and, as far as is possible, can be derived from theoretical calculations or from experimental results. The term *mesoscopic* is used to distinguish between the approach outlined in this contribution from a simple description of kinetics, i.e. power-law kinetics or Hougen–Watson rate expressions, and the surface science approach introduced by the ICI group [4,5] and the Topsøe group [6–16]. The surface science approach aims at obtaining an exact microscopic description of the kinetics in terms of molecular properties, i.e. the translational, vibrational, and rotational states of surface adsorbates using statistical mechanics. Fig. 1 displays the interplay of the most important data required for microkinetic analysis. In general, kinetic studies under ultrahigh vacuum conditions on single crystals provide important information on the kinetics of the elementary reaction steps on well-defined surfaces. From these studies the surface of a working catalyst under operating

* Fax.: +49-2-34-700-6745
E-mail address: olaf@techem.ruhr-uni-bochum.de (O. Hinrichsen)

0920-5861/99/$ – see front matter
PII: S0920-5861(99)00115-7

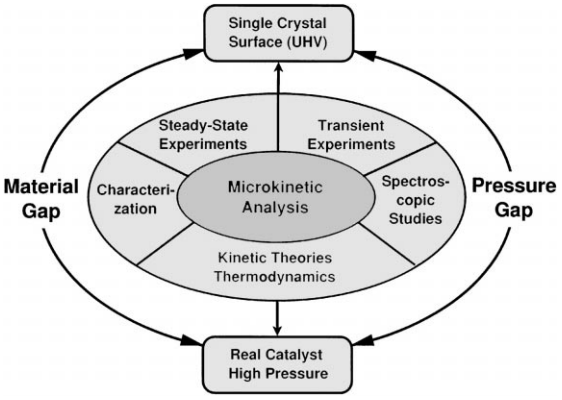

Fig. 1. The role of microkinetic analysis.

conditions might be described (*material gap*) [17]. Furthermore, by use of microkinetic analysis it might be possible to bridge the *pressure gap* between experimental conditions in UHV and under high pressure. The experimental results obtained under transient and steady-state operation on a catalyst under working conditions serve as starting point in the microkinetic analysis. Characterization methods provide valuable information about the morphology, BET area, specific surface area, and pore structure of a heterogeneous catalyst. By means of spectroscopic techniques, the existence and stability of static and reactive surface intermediates can be evaluated. Furthermore, kinetic theories and thermodynamics, e.g. the kinetic theory of gases and transition state theory (TST), are used to establish microkinetic models which are able to describe experiments under UHV and high pressure reaction conditions and can be applied by extrapolation over a wide range of experimental reaction conditions.

Much effort in the fields of microkinetic analysis has been done by Dumesic and his co-workers [3], who describe the theoretical concepts used for microkinetic analysis in their book in great detail. Seven catalytic systems, including metals, oxides, acids and zeolites are discussed as examples: ethylene hydrogenation catalyzed by platinum [18,19], ammonia synthesis catalyzed by iron (based on the results of Bowker et al. [4,5] and Stoltze and Nørskov [6–12,20]), ethane hydrogenolysis catalyzed by group VIII metals, methane oxidation catalyzed by molybdenum and vanadium oxides, methane dimerization catalyzed by Li-MgO, redox catalysis by transition metals exchanged in zeolites, isobutane cracking catalyzed by acid zeolites which has been studied by Yaluris et al. [21,22] in more detail. In further studies, microkinetic analysis has been applied by the Dumesic group to the dehydrogenation of isobutane catalyzed by supported Pt catalysts [23–25].

Alkali-promoted Ru-based catalyst have the potential to become the next generation of highly active low-pressure, low-temperature ammonia synthesis catalysts [26–29]. A promising candidate seems to be a ruthenium-carbon system promoted with alkali metal oxides or with oxides of alkaline earth metals [30,31]. Such a catalyst, based on thermally modified active carbon (high surface area graphite, HSAG), and promoted with cesium and barium [26] was introduced commercially in the Kellogg Advanced Ammonia Process (KAAP) [32,33]. This process allows for a reduction in energy costs due to the lower reaction pressure. In ongoing research at Engelhard on the optimization of this ammonia synthesis catalyst, data concerning the chemical composition, preparation procedure, and stability of the catalyst have, however, not been published so far. Over the last three decades, pioneering experimental work has been done by the group of Aika at the Research Laboratory of Resources Utilization Tokyo Institute of Technology. In their recent research works, Aika and co-workers have focussed on the preparation of Ru-based supported catalyst prepared from chlorine-free precursors [34–37] as well as from nitrido-ruthenium $[Ru_6]N$ clusters [38–40]. Moreover, NH_3 synthesis catalysts with lanthanide oxides used as the support, rather than as a dopant, showed a sufficiently high catalytic activity [41–43]. Recently, they prepared Ru catalysts supported on hydrogen-treated active carbon [44,45].

Rosowski et al. prepared Ru supported on magnesium oxide by using the alkali metal salt Cs_2CO_3 in a non-aqueous preparation method [46]. The Cs_2CO_3-Ru/MgO catalyst exhibited a remarkably enhanced catalytic activity as compared with either the conventionally prepared $CsNO_3$-Ru/MgO catalyst [36,46] or with the doubly promoted iron industrial catalyst Fe-Al_2O_3-K_2O. Recently, the work by Kowalczyk [47–50] has produced a promising ruthenium catalyst supported on a pre-calcined active carbon promoted with alkali metal compounds. A new class of ruthenium catalyst has also been obtained by the group of Shur [51,52] who used graphite-like active carbon as support for anionic metal carbonyl

clusters of ruthenium. A review of ammonia synthesis catalyzed by iron is given in [53,54].

2. Kinetic model formulation at mesoscopic level

2.1. Experimental

The kinetic experiments were carried out in glass-lined fixed-bed reactors positioned in a flow system built out of stainless steel which could be operated at pressures up to 100 bar. Further details are described in [46,55,56]. High purity gases were used in order to prevent the catalyst from poisoning. Heat or mass transport limitations were avoided by using 0.1–0.2 g of the 250–800 μm sieve fraction for the kinetic experiments, resulting in bed heights of a few millimeters [57,58]. The kinetics of Ru supported on Al_2O_3 (Ru/Al_2O_3), on MgO (Ru/MgO) and Ru/MgO promoted with cesium (Cs-Ru/MgO) have been studied [46]. Data acquisition of the effluent NH_3 mole fraction was performed by means of a sensitive infrared absorption detector. Transient experiments require a rapid on-line detection, and in our studies, gas analysis was performed by a quadrupole mass spectrometer (Balzers GAM 445) which was calibrated with binary reference gas mixtures. Details regarding the preparation and the characterization of the Ru-based catalysts by means of N_2 physisorption, static H_2 chemisorption, transmission, electron microscopy (TEM), X-ray diffraction (XRD), and electron spectroscopy (XPS and UPS) are given in [46,59].

Generally, the reduction was carried out in stoichiometric H_2/N_2 synthesis gas under atmospheric pressure with a heating rate of $0.5\,K\,min^{-1}$ up to 773 K. Kinetic steady-state experiments were performed by varying the feed gas composition and the space time, τ, in the pressure range of 0.1–5.0 MPa either by cycling the temperature in a range within 450 and 773 K or in a temperature-scanning mode [46]. Prior to each transient experiment, the steady-state ammonia synthesis activity was measured in order to achieve a well-defined starting point. The procedure for the temperature-programmed experiments and the isotopic exchange reaction (IER) have been published elsewhere in more detail [56,58,60,61].

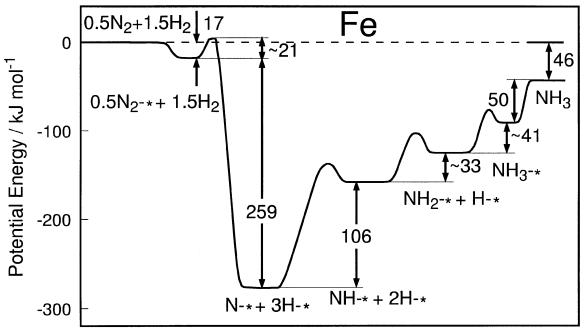

Fig. 2. One-dimensional potential energy diagram illustrating the progress of ammonia synthesis on iron; energies are in kJ/mol (after Ertl [73])

2.2. Microkinetic model

Using surface science techniques, Ertl and co-workers [62–69] studied ammonia synthesis under UHV conditions on clean Fe and potassium-promoted Fe single crystal surfaces. The experimental work comprised the determination of the kinetic parameters, i.e. sticking probabilities, activation energy of ad/desorption, and the preexponential factor for desorption. Finally, they constructed a reaction mechanism based on elementary steps with a complete one-dimensional potential-energy diagram for the synthesis of ammonia over the iron catalyst, as shown in Fig. 2 [70–73]. The formation of ammonia occurs via the dissociative chemisorption of nitrogen from a di-σ bound molecular chemisorbed α-N_2-∗ species with stepwise subsequent hydrogenation of atomic adsorbed hydrogen forming the intermediates NH-∗, NH_2-∗, and NH_3-∗ in succession. The following sequence of elementary steps can be written down for the overall reaction:

$$N_2 + * \rightleftharpoons N_2\text{-}* \quad (1)$$

$$N_2\text{-}* + * \rightleftharpoons 2N\text{-}* \quad (2)$$

$$N\text{-}* + H\text{-}* \rightleftharpoons NH\text{-}* + * \quad (3)$$

$$NH\text{-}* + H\text{-}* \rightleftharpoons NH_2\text{-}* + * \quad (4)$$

$$NH_2\text{-}* + H\text{-}* \rightleftharpoons NH_3\text{-}* + * \quad (5)$$

$$NH_3\text{-}* \rightleftharpoons NH_3 + * \quad (6)$$

$$H_2 + 2* \rightleftharpoons 2H\text{-}* \quad (7)$$

The $*$ designates a free active site at the catalyst surface and X-$*$ an adsorbed species. Based on the work from Ertl and co-workers, the research groups of Bowker et al. [4,5] and of Stoltze and Nørskov [6–12] constructed microkinetic models for ammonia synthesis. A detailed comparison of the microkinetic models of both research groups has been presented by Dumesic and Treviño [74]. They could show that the kinetic expressions with parameters taken from studies on single crystal surfaces collected under UHV conditions could describe the high-pressure kinetics observed on a multiply promoted industrial iron catalyst, i.e. bridging a pressure gap of about 10 to 12 orders of magnitude. The success of the microkinetic models is based on the fact that these describe correctly the kinetically significant elementary step of the overall reaction at a *mesoscopic* level. However, there is still a dispute in the literature as to the validity of the models of the research groups due to the difference in the activation barrier of dinitrogen dissociation [54,74–78]. Recently, Alstrup et al. [79,80] measured the sticking probability of nitrogen on Fe(111) in a UHV chamber under elevated pressure. Their results suggest that the dissociative chemisorption of N_2 proceeds via a precursor-mediated rather than a direct, activated process. Furthermore, density functional theory (DFT) calculations of the energetics of N_2 adsorption and dissociation on a Fe(111) surface by Mortensen et al. [81] might help to elucidate the kinetics of dissociative dinitrogen chemisorption on a catalyst under working conditions.

A reaction mechanism for ruthenium was independently confirmed by several research groups, including Danielson et al. [82,83], Egawa et al. [84,85], Tsai and Weinberg [86,87] and by the Ertl group [88–94]. The latter group carried out extensive experimental and theoretical work on Ru(0001), Ru($10\bar{1}0$) and Ru($11\bar{2}1$) surfaces comprising studies on the dissociative chemisorption of N_2 [89–91,94], the chemisorption and interaction of hydrogen with nitrogen [88,95], and the decomposition kinetics of NH_3 [93,96]. Therefore, a mechanism through the formation of a dehydrodiimide proposed by Fastrup [97] should be ruled out. Contrary to Fe, there is no indication for a molecularly chemisorbed N_2-$*$ for the dissociation of dinitrogen on Ru single crystal surfaces. Hence the dissociation step is written in one equation in the complete reaction mechanism:

$$N_2 + 2* \rightleftharpoons 2N\text{-}* \tag{8}$$

2.3. Modeling and simulation

In our kinetic simulation of the steady-state kinetics, we have modeled the plug-flow reactor by a series of well-mixed isothermal cells assuming that the temperature everywhere in the reactor is constant and that the temperature of all reaction intermediates is well-defined and identical [58]. In each cell, the steady-state equations for all surface intermediates, the site balance on the catalyst surface, and the material balances for the gaseous species were solved without any a priori assumptions regarding possible rate determining steps (RDS) or most abundant reaction intermediates (MARI) [98].

Modeling the transient experiments transforms the algebraic equations into differential equations. The resulting system of nonlinear differential-algebraic equations consists of the non-steady-state equations for all surface intermediates, the site balance on the catalyst surface and the material balances for the gaseous species. This set of equations was solved numerically without assuming a rate-determining step using the software package DDASAC (Double Precision Differential-Algebraic Analysis Sensitivity Code) for the ordinary differential equations, and PDASAC (Double Partial-Differential-Algebraic Analysis Sensitivity Code) for the partial differential equations. Both packages were developed by Stewart et al. [99] and turned out to be very useful for solving reaction-diffusion problems in catalytic reactors. For the PDEs, using spatial discretization, the system reduces to a set of nonlinear ordinary differential-algebraic equations (Method of lines). The ODEs could be also solved by a variable-order, variable-step method implementing the backward differentiation formula (BDF) which can be taken from the NAG library [100]. For the temperature-programmed experiments, the influence of the degree of backmixing was studied by applying either the continous stirred tank reactor (CSTR) model under conditions of perfect mixing or the PFR model as the two limiting cases within a microreactor for the design equation. The results have been presented in more detail elsewhere [58,101].

The optimization program used for the determination of the insignificant kinetic parameters, i.e. $A_{i,\mathrm{for}}$,

$A_{i,\mathrm{rev}}$, $E_{i,\mathrm{for}}$ and $E_{i,\mathrm{rev}}$ is similar to that described by Dumesic et al. [102], combined with the Generalized Regression Software (GREG) developed by Stewart et al. [99] and a Nonmonotonic Nonlinear Equation Solver (NNES) developed by Bain [103]. An Arrhenius form of the elementary step rate constants without coverage-dependence kinetic parameters was used in the simple Langmuirian microkinetic model which justifies the *mesoscopic* level of modeling. In addition, the NH_3 mole fraction at the reactor exit at given reaction conditions (pressure p, temperature T, and volumetric flow rate Q) and the number of active sites S_R (which is equal to the specific active surface area) need to be further specified.

3. Results and discussion

3.1. Interaction of N_2 with Ru-based catalysts

The dissociative chemisorption of dinitrogen is a very slow process and, in turn, is accepted to be the rate-determining step (RDS) of ammonia synthesis over Fe- and Ru-based catalysts. While the initial dissociative sticking coefficient for N_2 on Fe single crystal surfaces lies in the range 10^{-8} to 10^{-6}, on Ru(0001), Ru($10\bar{1}0$) and Ru($11\bar{2}1$) surfaces, an extremely low initial sticking coefficient of $(1 \pm 0.8) \times 10^{-12}$ was measured at room temperature and was found to be independent of surface orientation [89,91]. Higher sticking coefficients have been observed by Matsushima [104] and Romm et al. [105] using molecular beam experiments ($s_0 > 10^{-8}$) and Shi et al. [95] using the hot filament of an ionization gauge for N_2 dissociation ($s_0 > 10^{-6}$). Recently, Dahl et al. [106] measured the rate of NH_3 formation over a ruthenium single crystal in a stainless steel UHV system at pressures up to 2 bar and in a temperature range 598–898 K. An Arrhenius plot of the rates of ammonia synthesis yielded an overall activation energy for the synthesis of 101 kJ/mol. Extrapolating to 300 K results in a sticking coefficient of 4×10^{-20}. The high difference in the sticking coefficients published could be explained by the high coverage of reaction intermediates during synthesis, presumably by the inhibiting effect of hydrogen [106].

On Ru-based catalysts, the interaction with N_2 was studied by performing temperature-programmed N_2 adsorption (N_2 TPA) and desorption (N_2 TPD) experiments and the isotopic exchange reaction (IER) of $^{14}N^{14}N + {}^{15}N^{15}N \rightleftharpoons 2\,{}^{14}N^{15}N$ in a microreactor flow system [56]. Ru/Al_2O_3, unpromoted Ru/MgO and Cs-Ru/MgO have been studied as model catalysts in order to explore the effect of the support and the role of the alkali promoter in NH_3 synthesis [60,107]. Ru/Al_2O_3 turned out to be rather inactive for N_2 dissociation. Even dosing pure N_2 at pressures up to 10 bar did not result in a complete saturation with adsorbed atomic nitrogen. However, saturation with N-$*$ was achieved on Ru/MgO and Cs-Ru/MgO by long-term dosing of nitrogen over the catalyst. The subsequent N_2 TPD profiles displayed in Fig. 3 clearly reflect the difference in the rates of N_2 desorption for the three catalysts. For lower initial surface coverages, the broad and symmetric N_2 desorption peak was observed to shift to higher temperatures as expected for second-order desorption without readsorption within the catalyst bed. The rate constant of the associative desorption of N_2, $k_{0,\mathrm{rev}}$, from Ru/MgO was derived from TPD experiments with different heating rates yielding $A_{0,\mathrm{rev}} = 1.5 \times 10^{10}\,\mathrm{s}^{-1}$ and $E_{0,\mathrm{rev}} = 158$ kJ/mol. Furthermore, it was found that the TPD experiments from Ru/Al_2O_3 can be modeled with the same kinetic parameters assuming a maximum relative coverage of $\Theta_N = 0.25$. A better agreement between experimental and calculated data would be obtained by introducing coverage-dependent kinetic parameters, as shown in TPD study on a multiply promoted iron catalyst [77,78]. Tsai and Weinberg [86,87] and Shi et al. [95] have reported N_2 TPD profiles from Ru(0001) with in a single peak at a maximum of about 750 K (for a heating rate β of 10 K/s). When the preexponential factor and the activation energy for Ru/Al_2O_3 were used the simulation predicts a peak at 750 K in good agreement with experiments with Ru(0001). Due to the lower experimental peak position for Cs-Ru/MgO, the activation energy was lowered to $E_{0,\mathrm{rev}} = 137$ kJ/mol. This result can be explained by the existence of a highly and uniformly (Cs+O)-covered Ru metal surfaces [56].

The dissociation kinetics of N_2 were studied in more detail by exposing the catalysts to a dilute mixture of $^{14}N_2$ and $^{15}N_2$ in He in a temperature range 400 to 750 K. The following sequence in the isotopic exchange rate has been observed: Cs-Ru/MgO > Ru/MgO $\gg$ Ru/Al_2O_3. This experi-

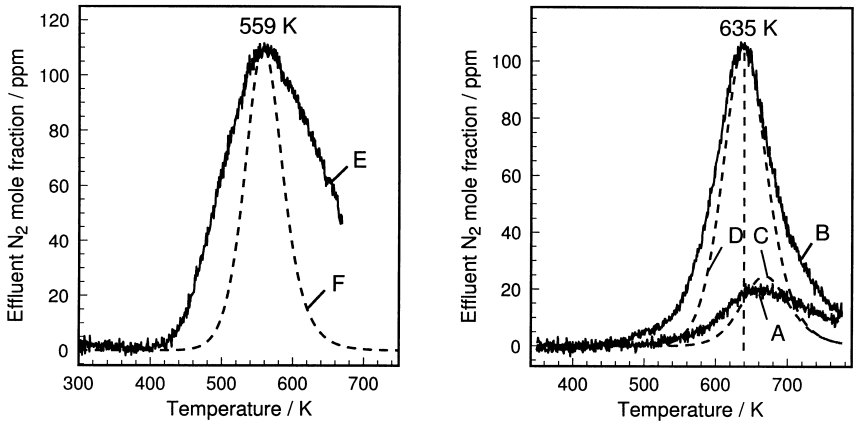

Fig. 3. Right half: Experimental N_2 TPD data (solid lines) for Ru/Al_2O_3 (trace A) and Ru/MgO (trace B). The TPD data were obtained by dosing N_2 at 573 K for 14 h and subsequent cooling in N_2 to room temperature. The heating rate β was 5 K/min in both experiments. Traces C and D (dashed lines) symbolize the modeling results using $k_{des} = 1.5 \times 10^{10}\,s^{-1} \times \exp(-158\,kJ/mol/RT)$ with initial condition Θ_N =0.25 for Ru/Al_2O_3 (trace C) and Θ_N =1.0 for Ru/MgO (trace D).Left half: Experimental N_2 TPD data (solid lines) for Cs-Ru/MgO. The TPD data were obtained by cooling in a flow of 50 Nml/min N_2 from 673 K to 298 K. β was chosen to be 1 K/min (trace E). The modeled TPD trace F using $k_{des} = 2.0 \times 10^{10}\,s^{-1} \times \exp(-137\,kJ/mol/RT)$ is shown as dashed line and was scaled in height.

ment helped to determine $k_{0,for}$ when $k_{0,rev}$ has been derived independently from TPD experiments. Microkinetic analysis of the IER experiments yielded a $A_{0,for} = 56(kPa\,s)^{-1}$ and $E_{0,for} = 33$ kJ/mol and 48 kJ/mol for Cs-Ru/MgO and Ru/MgO, respectively. The $E_{0,for}$ of 60 kJ/mol for Ru/Al_2O_3 could be regarded as an initial estimate of the activation energy.

The N_2 chemisorption kinetics were obtained independently from the desorption kinetics by flowing a dilute mixture of N_2 in He through the catalyst bed while increasing the temperature linearly (temperature-programmed N_2 adsorption (N_2 TPA)). For Cs-Ru/MgO, it was possible to predict the TPA peak shape and its position at 380 K based on the rate constants derived from the N_2 TPD and IER experiments. At higher temperatures, more active sites seem to be present which may be ascribed to the presence of a two-dimensional fluid–solid equilibrium of the (Cs +O)-coadsorbate layer. Ru/MgO turned out to be a heterogeneous system because of the existence of two TPA peaks [56]. The existence of a second active site was further identified by a small additional TPD peak at lower temperatures and by the same onset temperature of $^{14}N^{15}N$ formation as for the Cs-promoted catalyst. Such promoted sites my originate from the interaction with oxygen vacancies in the alkaline earth support at the interface.

When the rate constant for N_2 dissociation on Ru/Al_2O_3 is used, the extrapolated sticking coefficient of about 10^{-15} at 300 K agrees with the inertness towards dissociative chemisorption of N_2 observed for Ru(0001) under UHV conditions [89]. Furthermore, density functional theory calculations done by Mortensen et al. [108,109] confirmed the extremely small sticking coefficient. The activation energy was found to be 131 kJ/mol. Since the surface should be covered to some extent by reaction intermediates during NH_3 synthesis a higher overall activation energy E_{app} should be expected than for the RDS. However, Dahl et al. [106] derive from steady-state NH_3 synthesis experiments on Ru(0001) at 2 bar a value of $E_{app} = 101$ kJ/mol which, in turn, is higher than the barrier of 60 kJ/mol for N_2 dissociation on the Ru/Al_2O_3 catalyst. The conflict between theoretical and experimental work gives rise to open questions and further investigations in the future.

3.2. Temperature-programmed hydrogenation reaction (TPSR)

The removal of preadsorbed atomic adsorbates from catalysts in a microreactor set-up by heating in a reactive gas stream can be used for the quantitative

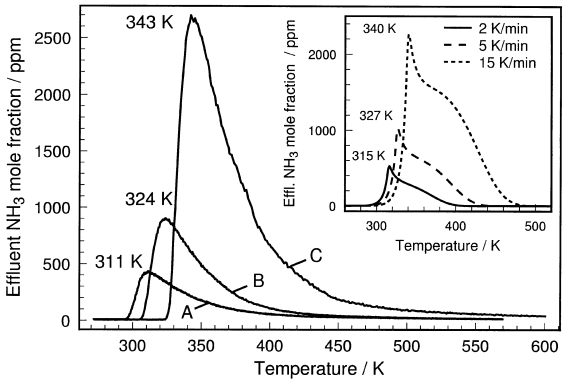

Fig. 4. Temperature-programmed surface reaction (TPSR) experiments. The heating rates were 2 K/min (trace A), 5 K/min (trace B), and 15 K/min (trace C). Saturation with atomic adsorbed nitrogen (N-∗) was achieved by dosing N_2 at 673 K for one hour and subsequent cooling in N_2 below room temperature. The inset shows the modeling results using Θ_N =0.95 as initial value.

determination of the coverage of the adsorbate. For the case of saturation, and a known adsorption stoichiometry, the derivation of the number of active sites S_R is straighforward. Fastrup et al. [55] conducted this transient technique for a N-∗ TPSR study (N-∗ +1.5 $H_2 \rightarrow NH_3$ +∗) with a multiply promoted iron catalyst under atmospheric pressure. Performing this titration experiment in a temperature-programmed way instead of under isothermal conditions has the advantage that significantly more information about the rate of the surface reaction is available [110–112]. In general, the shape of the TPSR profiles are strongly influenced by the reaction parameters, (p, T, Q, and β) as well as by the presence of coadsorbates [101]. Experiments using different heating rates and various initial coverages of adsorbates lead to TPSR profiles exhibiting a different peak shape and peak position. The evaluation of the experimental results aided by computer simulation provides an understanding of the kinetics of the elementary steps involved in the surface reaction.

The experimental TPSR data for Cs-Ru/MgO obtained after saturation with atomic adsorbed nitrogen are shown in Fig. 4. The low-temperature part of the TPSR profile demonstrates the autocatalytic kinetics of the surface reaction, preadsorbed atomic nitrogen is quickly hydrogenated stepwise to NH_3-∗. The desorption of NH_3 creates free surface sites for the dissociative adsorption of H_2 resulting in an increasing coverage of H-∗ which, in turn, accelerates the hydrogenation of N-∗. The sharp onset and the maximum of the signals were found to shift using 2 K/min (trace A), 5 K/min (trace B), 15 K/min (trace C) to higher temperatures (T_{max} =311 K, 324 K, and 343 K, respectively). The integration of the experimental traces yielded 24.5 μmol/g corresponding to 24.5 μmol/g active sites for ammonia synthesis assuming a stoichiometry of 1/1 for N-∗/active site (∗). The inset shows the calculated profiles which are considered to be in good agreement concerning the onset temperature, the sharpness of the onset, the maxima of the signals, and the high-temperature tailing. Kinetic simulations showed only minor changes in the results depending on the reactor model employed [101]. For Ru/MgO, $E_{2,for}$ was increased by 25 to 111 kJ/mol in order agree with the experimental shift of the onset temperature and the signal maxima to higher temperatures. Based on the assumption that the surface is rapidly saturated by H-∗ and that the reaction N-∗ +3 H-∗ → NH_3 + 4∗ obeys quasi first-order kinetics, an Arrhenius-type plot of $\ln(T_{max}^2/\beta)$ versus $1/T_{max}$ yields an apparent activation energy of 86 kJ/mol which is in good agreement with the 93 kJ/mol derived for unpromoted Ru(0001) by Shi et al. [88].

3.3. Ammonia synthesis

It is well-known from the literature that unpromoted ruthenium powder is rather inactive in NH_3 [26,113,114]. Rosowski et al. [46] present a detailed kinetic study for Ru-based catalysts under industrial synthesis conditions. The following sequence with respect to the turnover frequency r^{TOF} of NH_3 formation was found: Cs_2CO_3-Ru/MgO > $CsNO_3$-Ru/MgO > Ru/MgO > Ru/K-Al_2O_3 > Ru/Al_2O_3 with a r^{TOF} ranging from 10^{-4} to 10^{-1}/s which is based on H_2 chemisorption and strongly depends on the chosen reaction conditions. With the Cs-promoted Ru/MgO catalysts a higher catalytic activity was observed than for a multiply promoted Fe catalyst at atmospheric pressure. An initial r^{TOF} of approximately 10^{-2}/s is obtained for the non-aqueously prepared Cs_2CO_3-Ru/MgO catalyst at 588 K. Ammonia synthesis turnover frequencies were reported by Dahl et al. [106] on Ru(0001) to be 2×10^{-2}/s at 673 K. However, Rosowski et al. [46] published a r^{TOF} of

7×10^{-4}/s for Ru/Al_2O_3 which is considered to correspond to unpromoted Ru. Unfortunately, both r^{TOF} are not comparable because of the higher flow rate, and a higher partial pressure of ammonia formed, and the uncertainty in counting active sites [115] which may account for a lower r^{TOF} in the case of Ru/Al_2O_3.

All the information from the aforementioned experiments (N_2 TPA, N_2 TPD, IER, and N-$*$ TPSR) combined with the kinetic data collected under steady-state operations were integrated into a microkinetic model for Cs-Ru/MgO. The missing kinetic parameters have been taken as starting values from surface science studies [87]. Table 1 lists the values of $k_{i,\text{for}}$ and $k_{i,\text{rev}}$ obtained after optimization in the case of Cs-Ru/MgO.

Microkinetic models have to be consistent with the overall reaction thermodynamics. For all independent reaction paths through the mechanism from reactants to products the sum of the activation energies and the products of the preexponential factors must equal the heat of the net reaction, which is related to the standard entropy change for the net reaction [3]:

$$\sum_i \sigma_i(E_{i,\text{for}}) - \sigma_i(E_{i,\text{rev}} = \Delta H^0_{\text{net}}$$

$$\prod_i \left(\frac{A_{i,\text{rev}}}{A_{i,\text{for}}}\right)^{\sigma_i} = \exp\left(\frac{\Delta G^0_{\text{net}} - \Delta H^0_{\text{net}}}{\mathrm{R}\,T}\right)$$

where σ_i are the stoichiometric numbers of the elementary steps in the reaction path, ΔH^0_{net} and ΔG^0_{net} are the standard enthalpy and Gibbs free energy changes of the net reaction. Therefore, the product of the equilibrium constants for the elementary steps must yield the overall equilibrium constant for the stoichiometric reaction. At a temperature of 723 K, the overall equilibrium constant for forming 2 mol of NH_3 was predicted to be 5×10^{-9} $(\text{kPa})^{-2}$ in exact agreement with the experimental value.

The results of all simulations of the steady-state kinetics showed that indeed the dissociation of dinitrogen (step 0) is the RDS of the overall reaction. A potential-energy diagram for the progress of the synthesis of ammonia catalyzed by Cs-Ru/MgO can be constructed from the activation energies of the elementary steps (Fig. 5). Kinetic simulations have been performed over a wide range of reaction conditions [61]. The parity plot in Fig. 6 demonstrated the very good agreement of the calculated NH_3 mole fraction x_{NH_3} at the reactor exit with the measured data points. Data

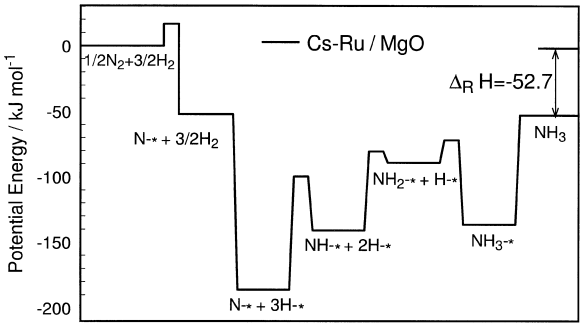

Fig. 5. Schematic energy profile of the progress of ammonia synthesis catalyzed by with Cs-Ru/MgO; energies are in kJ/mol.

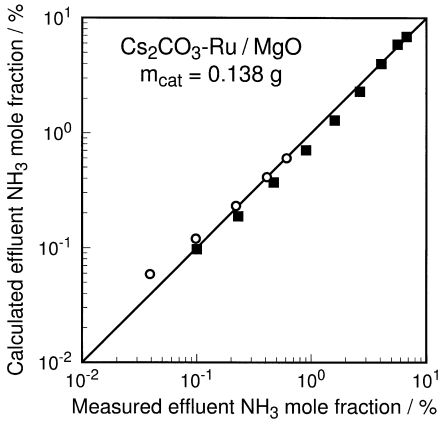

Fig. 6. Comparison of effluent NH_3 mole fraction measured with Cs-Ru/MgO over a wide range of experimental reaction conditions (open dot: p =0.1 MPa, full squares: p =5.0 MPa) against the corresponding data calculated with the microkinetic model listed in Table 1 (data are taken from the work of Rosowski et al. [46] and Hinrichsen [61])

points far from equilibrium have been included in the figure in order to provide a good test of the ammonia synthesis microkinetic model.

The fractional surface coverages, Θ_i, of the predominant adsorbed species, i.e. H-$*$, N-$*$, and NH_3-$*$, are plotted versus the dimensional longitudinal distance along the plug-flow reactor in Fig. 7. In contrast to high-pressure ammonia synthesis catalyzed by iron where the MARI is adsorbed atomic nitrogen except at the reactor inlet, here the nature of the MARI depends strongly on the position of the catalyst in the reactor. Under high pressure the surface at the reactor outlet predominantly consists of atomic adsorbed hydrogen at low temperature, while near reaction temperature a variety of adsorbed species compete for free active sur-

Table 1
Rate constants of the elementary steps in the microkinetic model of ammonia synthesis catalyzed by Cs-Ru/MgO; $*$ $(\mathrm{kPa\,s})^{-1}$ for forward reaction of step 0 and 6 as well as reverse reaction of step 5, s^{-1} for all other elementary reaction

elementary step	Forward rate constant		Reverse rate constant	
	preexponential factor $A_{i,\mathrm{for}}$	activation energy $E_{i,\mathrm{for}}$ (kJ/mol)	preexponential factor $A_{i,\mathrm{rev}}$	activation energy $E_{i,\mathrm{rev}}$ (kJ/mol)
$N_2 + 2* \rightleftharpoons 2N*$	$5.6 * 10^{1}$	33.0	$2.0 * 10^{10}$	137.0
$N* + H* \rightleftharpoons NH* + *$	$6.0 * 10^{13}$	86.5	$2.8 * 10^{14}$	41.2
$NH* + H* \rightleftharpoons NH_2* + *$	$4.7 * 10^{13}$	60.4	$1.8 * 10^{13}$	8.6
$NH_2* + H* \rightleftharpoons NH_3* + *$	$3.3 * 10^{13}$	17.2	$9.3 * 10^{12}$	64.6
$NH_3* \rightleftharpoons NH_3 + *$	$5.9 * 10^{13}$	83.7	$2.1 * 10^{6}$	0.0
$H_2 + 2* \rightleftharpoons 2H*$	$5.5 * 10^{5}$	0.0	$2.3 * 10^{13}$	89.4

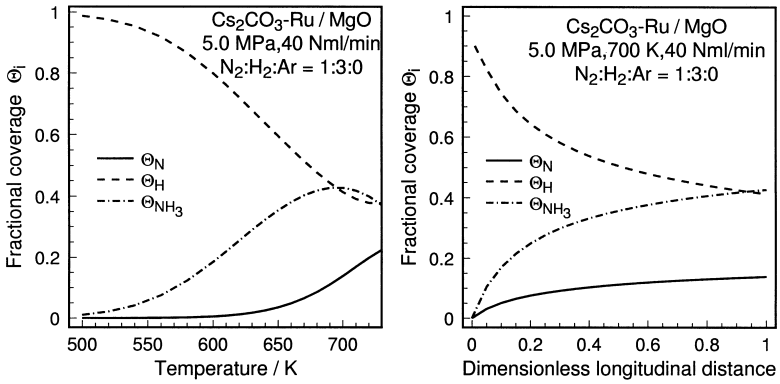

Fig. 7. Left half: Calculated fractional coverages Θ_H, Θ_N, and Θ_{NH_3} at reactor exit versus reaction temperature under high pressure using a stoichiometric feed gas. Right half: Calculated fractional coverages Θ_H, Θ_N, and Θ_{NH_3} vs. dimensional longitudinal distance from the reactor inlet under constant reaction conditions.

face sites (left half). Correspondingly at constant reaction temperature, the coverage of H-$*$ drops from the inlet of the plug-flow reactor while the amount of adsorbed N-$*$ and NH_3-$*$ increases. Under atmospheric pressure, the surface composition changes slightly to a higher fractional coverage of N-$*$.

Compared to the NH_3 synthesis catalyzed by iron, the interaction of hydrogen is significantly stronger with ruthenium than with iron. Obviously, hydrogen blocks active surface sites, and corespondingly inhibits ammonia formation. This conclusion is confirmed by kinetic simulations shown in Fig. 8, where the NH_3 effluent mole fraction is plotted versus the dimensional longitudinal distance varying the feed gas composition. Indeed, experimental evidence was found by Rosowski et al. [46], who derived from power-law kinetics a negative reaction order for hydrogen and obtained a significant higher catalytic activity under

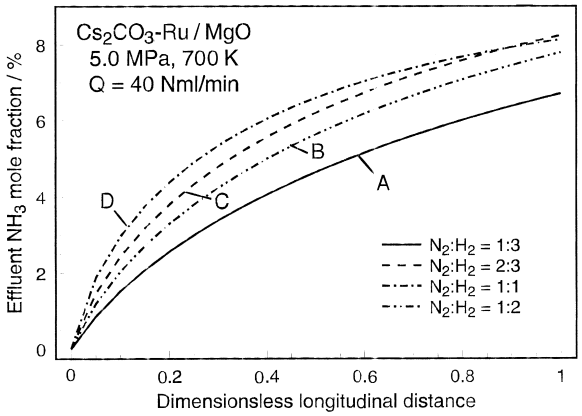

Fig. 8. Dependence of the effluent mole fraction of ammonia x_{NH_3} versus dimensional longitudinal distance from the reactor inlet on the feed gas composition (A): $N_2 : H_2 = 1 : 3$, (B) $N_2 : H_2 = 1 : 2$, (C) $N_2 : H_2 = 2 : 3$, and (D) $N_2 : H_2 = 1 : 1$ calculated for Cs_2CO_3-Ru/MgO under constant reaction conditions.

high-pressure ammonia synthesis conditions using a non-stoichiometric feed gas composition with a lower H/N ratio. In agreement with the results of Rosowski et al., Tennison proposed a lower H/N ratio for commercial operation in his review on alternative non-iron catalysts for ammonia synthesis [26].

4. Conclusions

Based on extensive kinetic studies done by several research groups in the past decades, ruthenium-based catalysts have turned out to be a commercially promising alternative to the multiply promoted magnetite catalysts used for ammonia synthesis. Long-term stability and activity tests and further optimization of the existing catalyst concerning ruthenium loading, of the promoter type and loading, and of the support type will provide valuable information on the use of this new class of low-pressure, low-temperature NH_3 synthesis catalysts. Of particular interest are Ru catalysts supported on magnesium oxide or active carbon, both added with alkali or alkaline earth metal promoters.

Microkinetic modeling at mesoscopic level has been applied to study the effect of the support and the role of the alkali promoter of Ru-based catalysts used for high-pressure NH_3 synthesis. The combination of a wide variety of experimental techniques, which give further insight into the microscopic processes at the catalyst surface, results in microkinetic models, which reflect the experimental results. Compared to the iron catalysts, Ru catalysts demonstrate different industrial operating characteristics in terms of the H/N ratio response. The dissociation of dinitrogen is the rate-determining step in NH_3 synthesis, resulting in a lower coverage of atomic adsorbed nitrogen on the surface under industrial operationg conditions. The formation of NH_3 is strongly inhibited by hydrogen. Furthermore, it was possible to describe experimental results obtained with Ru single crystal surfaces under UHV conditions and elevated pressures as well as the performance of a ruthenium catalyst working at industrial reaction conditions, bridging the *pressure* and *material gaps*.

Why then, does this simple Langmuirian model work so well for NH_3 synthesis catalyzed by ruthenium? In general, Langmuirian kinetics are not expected to apply over a wide range of surface coverages. However, since the microkinetic model describes properly the kinetics and thermodynamics of nitrogen adsorption, it is effective in predicting the steady-state ammonia synthesis kinetics over a wide range of reaction conditions. It could further be demonstrated that the model over-estimates the performance of a transient experiment at critical surface coverages, i.e. at very high and at very low coverages. Nevertheless, with respect to the non-Langmuirian behavior, a coverage-dependence included into the rate constant of the elementary steps yields a better agreement between experimental and calculated data.

5. Notation

$A_{i,\mathrm{for}}$	pre-exponential factor of the forward rate constant of elementary step i $(\mathrm{kPa\,s})^{-1}$, s^{-1}
$A_{i,\mathrm{rev}}$	pre-exponential factor of the reverse rate constant of elementary step i $(\mathrm{kPa\,s})^{-1}$, s^{-1}
$E_{i,\mathrm{for}}$	activation energy of forward rate constant of elementary step i, kJ/mol
$E_{i,\mathrm{rev}}$	activation energy of reverse rate constant of elementary step i, kJ/mol
$k_{i,\mathrm{for}}$	forward rate constant of elementary step i $(\mathrm{kPa\,s})^{-1}$, s^{-1}
$k_{i,\mathrm{rev}}$	reverse rate constant of elementary step i $(\mathrm{kPa\,s})^{-1}$, s^{-1}
p	pressure, Pa
Q	volumetric flow rate, Nml/min
S_R	amount of active sites,μmol/g
R	gas constant, 8.314 J/K mol
r	reaction rate, μmol/ (s g)
r^{TOF}	turnover frequency, s^{-1}
s_0	initial sticking coefficient, –
T	temperature, K
w	catalyst weight, g
x_i	mole fraction of the gaseous species i, –
β	heating rate, K/min
Θ_i	fractional coverage of adsorbed species i, –
τ	space time, h^{-1}

Acknowledgements

The author would like to thank M. Muhler and his former co-workers at the FHI where much of the work was done. The author benefitted from fruitful discus-

sions with G. Ertl, R. Schlögl, K. Jacobi, K.-I. Aika, and S.R. Tennison. Furthermore, the author would like to thank J.A. Dumesic and R.D. Cortright for their help and discussions during his visit at the University of Wisconsin. Some results are obtained by means of the optimization software developed by W.E. Stewart.

References

[1] H. Bakemeier, T. Huberich, R. Krabetz, W. Liebe, M. Schunck, D. Mayer, in: Ammonia, 5.ed., Ullmann's Encyclopedia of Industrial Chemistry, 1997 CD ROM.
[2] M. Appl, Ammonia, Principles and Industrial Practice, Wiley-VCH, Weinheim, 1999.
[3] J.A. Dumesic, D.F. Rudd, L.M. Aparicio, J.E. Rekoske, A.A. Treviño, The Microkinetics of Heterogeneous Catalysis, ACS Professional Reference Book, Washington, DC, 1993.
[4] M. Bowker, I.B. Parker, K.C. Waugh, Appl. Catal. 14 (1985) 101.
[5] M. Bowker, I.B. Parker, K.C. Waugh, Surf. Sci. 197 (1988) L223.
[6] P. Stoltze, J.K. Nørskov, Phys. Rev. Lett. 55 (1985) 2502.
[7] P. Stoltze, J.K. Nørskov, J. Vac. Sci. Technol. A 5 (1987) 581.
[8] P. Stoltze, Physica Scripta 36 (1987) 824.
[9] P. Stoltze, J.K. Nørskov, Surf. Sci. 197 (1988) L230.
[10] P. Stoltze, J.K. Nørskov, J. Catal. 110 (1988) 1.
[11] P. Stoltze, J.K. Nørskov, Top. Catal. 1 (1994) 253.
[12] P. Stoltze, in: A. Nielsen (Ed.), Ammonia: Catalysis and Manufacture, 1st ed., Springer, Berlin, 1995, p.17.
[13] C.V. Ovesen, P. Stoltze, J.K. Nørskov, C.T. Campbell, J. Catal. 134 (1992) 445.
[14] T.S. Askgaard, J.K. Nørskov, C.V. Ovesen, P. Stoltze, J. Catal. 156 (1995) 229.
[15] C.V. Ovesen, B.S. Clausen, B.S. Hammershøi, G. Steffensen, T. Askgaard, I. Chorkendorff, J.K. Nørskov, P.B. Rasmussen, P. Stoltze, P. Taylor, J. Catal. 158 (1996) 170.
[16] C.V. Ovesen, B.S. Clausen, J. Schiøtz, P. Stoltze, H. Topsøe, J.K. Nørskov, J. Catal. 168 (1997) 133.
[17] P.L.J. Gunter, J.W. Niemantsverdriet, F.H. Ribeiro, G.A. Somorjai, Catal. Rev.-Sci. Eng. 39 (1997) 77.
[18] R.D. Cortright, S.A. Goddard, J.E. Rekoske, J.A. Dumesic, J. Catal. 127 (1991) 342.
[19] J.E. Rekoske, R.D. Cortright, S.A. Goddard, S.B. Sharma, J.A. Dumesic, J. Phys. Chem. 96 (1992) 1880.
[20] L.M. Aparicio, J.A. Dumesic, Top. Catal. 1 (1994) 233.
[21] G. Yaluris, J.E. Rekoske, L.M. Aparicio, R.J. Madon, J.A. Dumesic, J. Catal. 153 (1995) 54.
[22] G. Yaluris, J.E. Rekoske, L.M. Aparicio, R.J. Madon, J.A. Dumesic, J. Catal. 153 (1995) 65.
[23] R.D. Cortright, J.A. Dumesic, J. Catal. 148 (1994) 771.
[24] R.D. Cortright, J.A. Dumesic, J. Catal. 157 (1995) 576.
[25] R.D. Cortright, E. Bergene, P. Levin, M. Natal-Santiago, J.A. Dumesic, Stud. Surf. Sci. Catal. 101 (1996) 1185.
[26] S.R. Tennison, in: J.R. Jennings (Ed.), Catalytic Ammonia Synthesis, 1st ed., Plenum Press, New York, 1991, p. 303.
[27] T.A. Czuppon, S.A. Knez, R.V. Schneider III, G. Worobets, March, in: Presented at the 1993 AICHE Ammonia Safety Symp., September 1993, Orlando, FL. Chem. Eng. 100 (3) (1993) 19.
[28] A.K. Rhodes, Oil and Gas J. 11 (1996) 37.
[29] S.R. Tennison, in: Exciting trends in tuthenium and related catalysis, Y. Izumi, K.-I. Aika, M. Anpo (Eds.), The 14th Int. Conf. on Catalysis, Taniguchi Foundation, 1995, p. 1.
[30] A.I. Foster, P.G. James, J.J. McCarroll, S.R. Tennison, US Patent 4,163,775 (1979) Aug. 7.
[31] J.J. McCarroll, S.R. Tennison, N.P. Wilkinson, US Patent 4,600,571 (1986) July 15.
[32] P.J. Shires, J.R. Cassata, B.G. Mandelik, C.P. van Dijk, US Patent 4,479,925 (1984) Oct. 30.
[33] G.S. Benner, J.R. Le Blanc, J.M. Lee, H.P. Leftin, P.J. Shires, C.P. van Dijk, US Patent 4,568,532 (1986) Feb. 4.
[34] S. Murata, K.-I. Aika, Appl. Catal. A 82 (1992) 1.
[35] S. Murata, K.-I. Aika, J. Catal. 136 (1992) 110.
[36] K. Aika, T. Takano, S. Murata, J. Catal. 136 (1992) 126.
[37] S. Murata, K.-I. Aika, J. Catal. 136 (1992) 118.
[38] Y. Izumi, K.-I. Aika, Chem. Lett. (1995) 137.
[39] Y. Izumi, K.-I. Aika, J. Phys. Chem. 99 (1995) 10336.
[40] Y. Izumi, K.-I. Aika, J. Phys. Chem. 99 (1995) 10346.
[41] Y. Kadowaki, K.-I. Aika, J. Catal. 161 (1996) 138.
[42] Y. Niwa, K .-I. Aika, Chem. Lett. (1996) 3.
[43] Y. Niwa, K.-I. Aika, J. Catal. 162 (1996) 1.
[44] Z. Zhong, K. Aika, Inorg. Chim. Acta 280 (1998) 183.
[45] Z. Zhong, K.-I. Aika, J. Catal. 173 (1998) 535.
[46] F. Rosowski, A. Hornung, O. Hinrichsen, D. Herein, M. Muhler, G. Ertl, Appl. Catal. A: General 151 (1997) 443.
[47] Z. Kowalczyk, S. Jodzis, J. Sentek, Appl. Catal. A: General 138 (1996) 83.
[48] Z. Kowalczyk, J. Sentek, S. Jodzis, R. Diduszko, A. Presz, A. Terzyk, Z. Kucharski, J. Suwalski, Carbon 34 (1996) 403.
[49] Z. Kowalczyk, J. Sentek, S. Jodzis, E. Mizera, J. Goralski, T. Paryjczak, R. Diduszko, Catal. Lett. 45 (1997) 65.
[50] Z. Kowalczyk, S. Jodzis, W. Rarog, J. Zielinski, J. Pielaszek, Appl. Catal. A: General 173 (1998) 153.
[51] S.M. Yunusov, V.A. Likholobov, V.B. Shur, Appl. Catal. A: General 158 (1997) L35.
[52] S.M. Yunusov, E.S. Kalyuzhnaya, H. Mahapatra, V.K. Puri, V.A. Likholobov, V.B. Shur, J. Mol. Catal. A: Chemical 139 (1999) 219.
[53] J.R. Jennings, Catalytic Ammonia Synthesis, 1st ed., (Plenum Press, New York, 1991).
[54] R. Schlögl, in: Handbook of Heterogeneous Catalysis, G. Ertl, H. Knözinger, J. Weitkamp (Eds.), vol. 4, VCH Verlagsgesellschaft, Weinheim, 1997, p. 308.
[55] B. Fastrup, M. Muhler, H.N. Nielsen, L.P. Nielsen, J. Catal. 142 (1993) 135.
[56] O. Hinrichsen, F. Rosowski, A. Hornung, M. Muhler, G. Ertl, J. Catal. 165 (1997) 33.
[57] C.N. Satterfield, Heterogeneous Catalysis in Industrial Practice, McGraw-Hill, New York, 1991.
[58] O. Hinrichsen, F. Rosowski, M. Muhler, G. Ertl, Stud. Surf. Sci. Catal. 109 (1997) 389.
[59] M. Muhler, F. Rosowski, O. Hinrichsen, A. Hornung, G. Ertl, Stud. Surf. Sci. Catal. 101 (1996) 317.

[60] F. Rosowski, O. Hinrichsen, M. Muhler, G. Ertl, Catal. Lett. 36 (1996) 229.
[61] O. Hinrichsen, F. Rosowski, M. Muhler, G. Ertl, Chem. Engng Sci. 51 (1996) 1683.
[62] F. Bozso, G. Ertl, M. Grunze, M. Weiss, Appl. Surf. Sci. 1 (1977) 103.
[63] F. Bozso, G. Ertl, M. Grunze, M. Weiss, J. Catal. 49 (1977) 18.
[64] F. Bozso, G. Ertl, M. Weiss, J. Catal. 50 (1977) 519.
[65] M. Grunze, F. Bozso, G. Ertl, M. Weiss, Appl. Surf. Sci. 1 (1978) 241.
[66] G. Ertl, N. Thiele, Appl. Surf. Sci. 3 (1979) 99.
[67] G. Ertl, S.B. Lee, M. Weiss, Surf. Sci. 111 (1981) L711.
[68] G. Ertl, S.B. Lee, M. Weiss, Surf. Sci. 114 (1982) 515.
[69] G. Ertl, S.B. Lee, M. Weiss, Surf. Sci. 114 (1982) 527.
[70] G. Ertl, Catal. Rev.-Sci. Eng. 21(2) (1980) 201.
[71] G. Ertl, J. Vac. Sci. Technol. A 1 (1983) 1247.
[72] G. Ertl, in: Kinetics of chemical processes on well-defined surfaces, J.R. Anderson, M. Boudart (Eds.), Catalysis, Science and Technology, vol. 4, Springer, Berlin, 1983, p. 209.
[73] G. Ertl, in: J.R. Jennings (Ed.), Catalytic Ammonia Synthesis, 1st ed., (Plenum Press, New York) (1991) p. 109.
[74] J.A. Dumesic, A.A. Treviño, J. Catal. 116 (1989) 119.
[75] B. Fastrup, J. Catal. 150 (1994) 345.
[76] B. Fastrup, Top. Catal. 1 (1994) 273.
[77] M. Muhler, F. Rosowski, G. Ertl, Catal. Lett. 24 (1994) 317.
[78] O. Hinrichsen, F. Rosowski, M. Muhler, Chem.-Ing.-Tech. 66 (1994) 1375.
[79] I. Alstrup, I. Chorkendorff, S. Ullmann, J. Catal. 168 (1997) 217.
[80] I. Alstrup, I. Chorkendorff, S. Ullmann, Z. Phys. Chem. NF 198 (1997) 123.
[81] J.J. Mortensen, L.B. Hansen, B. Hammer, J.K. Nørskov, J. Catal. 182 (1999) 479.
[82] L.R. Danielson, M.J. Dresser, E.E. Donaldson, J.T. Dickinson, Surf. Sci. 71 (1978) 599.
[83] L.R. Danielson, M.J. Dresser, E.E. Donaldson, D.R. Sandstrom, Surf. Sci. 71 (1978) 615.
[84] C. Egawa, S. Naito, K. Tamaru, Surf. Sci. 138 (1984) 279.
[85] C. Egawa, T. Nishida, S. Naito, K. Tamaru, J. Chem. Soc. Faraday Trans. 1 (1984) 1595.
[86] W. Tsai, W.H. Weinberg, J. Phys. Chem. 91 (1987) 5302.
[87] W. Tsai, Interactions of Ammonia with Platinum and Ruthenium Surfaces, Ph.D. thesis, California Institute of Technology, 1987.
[88] H. Shi, K. Jacobi, G. Ertl, J. Chem. Phys. 102 (1995) 1432.
[89] H. Dietrich, P. Geng, K. Jacobi, G. Ertl, J. Chem. Phys. 104 (1996) 375.
[90] H. Dietrich, K. Jacobi, G. Ertl, J. Chem. Phys. 105 (1996) 8944.
[91] K. Jacobi, H. Dietrich, G. Ertl, Appl. Surf. Sci. 121/122 (1997) 558.
[92] H. Dietrich, K. Jacobi, G. Ertl, J. Chem. Phys. 106 (1997) 9313.
[93] H. Dietrich, K. Jacobi, G. Ertl, Surf. Sci. 377/379 (1997) 308.
[94] S. Schwegmann, A.P. Seitsonen, H. Dietrich, H. Bludau, H. Over, K. Jacobi, G. Ertl, Chem. Phys. Lett. 264 (1997) 680.
[95] H. Shi, K. Jacobi, G. Ertl, J. Chem. Phys. 99 (1993) 9248.
[96] H. Dietrich, K. Jacobi, G. Ertl, Surf. Sci. 352/354 (1996) 138.
[97] B. Fastrup, Catal. Lett. 48 (1997) 111.
[98] M. Boudart, G. Djéga-Mariadassou, Kinetics of Heterogeneous Catalytic Reactions, 1st ed., Princeton University Press, Princeton, 1984.
[99] W.E. Stewart, M. Caracotsios, J.P. Sørensen, Computational Modelling of Reactive Systems Butterworth, Stoneham, England, in preparation.
[100] NAG Fortran Library edition, Numerical Algorithm Group, 256 Banbury Road, Oxford OX27DE and U.K.
[101] O. Hinrichsen, A. Hornung, M. Muhler, Chem. Eng. Technol., submitted for publication.
[102] J.A. Dumesic, A.A. Treviño, B.A. Milligan, L.A. Greppi, V.R. Balse, K.T. Sarnowski, C.E. Beall, T. Kataoka, D.F. Rudd, Ind. Eng. Chem. Res. 26 (1987) 1399.
[103] R.S. Bain, Nonmonotonic nonlinear equation solver, Ph.D thesis, University of Wisconsin-Madison, 1993.
[104] T. Matsushima, Surf. Sci. 197 (1988) L287.
[105] L. Romm, G. Katz, R. Kosloff, M. Asscher, J. Phys. Chem B 101 (1997) 2213.
[106] S. Dahl, P.A. Taylor, E. Törnquist, I. Chorkendorff, J. Catal. 178 (1998) 679.
[107] O. Hinrichsen, F. Rosowski, A. Hornung, M. Muhler, G. Ertl, J. Catal. 165 (1997) 33.
[108] J.J. Mortensen, Y. Morikawa, B. Hammer, J.K. Nørskov, Z. Phys. Chem. NF 198 (1997) 113.
[109] J.J. Mortensen, Y. Morikawa, B. Hammer, J.K. Nørskov, J. Catal. 169 (1997) 85.
[110] J.L. Falconer, J.A. Schwarz, Catal. Rev.-Sci. Eng. 25(2) (1983) 141.
[111] J.A. Schwarz, J.L. Falconer, Catal. Today 7 (1990) 1.
[112] S. Bhatia, J. Beltramini, D.D. Do, Catal. Today 7 (1990) 309.
[113] G. Rambeau, H. Amariglio, J. Catal. 72 (1981) 1.
[114] G. Rambeau, A. Jorti, H. Amariglio, J. Catal. 74 (1982) 110.
[115] M. Boudart, Chem. Rev. 95 (1995) 661.